Scientific Research Publishing

Open Journal of Physical Chemistry, 2023, 13, 13-28
https://www.scirp.org/journal/ojpc
ISSN Online: 2162-1977
ISSN Print: 2162-1969

Fabrication and Characterization of Lanthanide-TiO_2 Nanotube Composites

Khadijah M. Emran[1*], Hessah E. Alanazi[2]

[1]Department of Chemistry, College of Science, Taibah University, Madinah, KSA
[2]Department of Chemistry, College of Science and Art, Al Jouf University, Qurayyat, KSA
Email: *kabdalsamad@taibahu.edu.sa, h.enazi@ju.edu.sa

How to cite this paper: Emran, K.M. and Alanazi, H.E. (2023) Fabrication and Characterization of Lanthanide-TiO_2 Nanotube Composites. *Open Journal of Physical Chemistry*, **13**, 13-28.
https://doi.org/10.4236/ojpc.2023.132002

Received: January 15, 2023
Accepted: March 18, 2023
Published: March 21, 2023

Abstract

Titanium dioxide (TiO_2) doped with neodymium (Nd) and/or Gadolinium (Gd) rare-earth elements were fabricated into nanotubes via the hydrothermal method in a KOH solution and *in-situ* doping. Titanium dioxide nanotubes (TNTs) and *in-situ* Nd-doped and/or Gd-doped TNTs were characterized with transmission and scanning electron microscopy, energy-dispersive X-ray analysis, X-ray diffraction, Raman spectroscopy, and Fourier-transform infrared spectroscopy. Morphologies indicated a network of aggregated nanotubes. The phase and composition analyses revealed that the lanthanide TNTs had anatase phases with Nd and/or Gd nanoparticles in the TNT lattice. The nanoparticles were uniformly deposited on the surface because of hydroxyl groups on the TNT surfaces, resulting in a very high loading density. The outer diameter and the length of the TNTs increased with doping. The mechanisms for the formation of multiwall TNTs are discussed.

Keywords

TiO_2 Nanotube, Lanthanide Doped, Hydrothermal, XRD, TEM, Raman Spectroscopy

1. Introduction

In the effort to improve the performance of fuel cells, dye-sensitized solar cells [1], photocatalysis [2] [3], and solar driven processes [4], the fabrication and electrocatalytic properties [5] [6] of metals deposited on nanomaterials have been intensely investigated. Nanoscale materials derived from titanium oxide (TiO_2) have been extensively investigated for various applications, including solar-cells and batteries [7] [8], hydrogen generation [9] [10] [11], drug delivery [12] [13], photolysis [14] [15], and electrocatalysis [16] [17]. Titanium nanotubes (TNT)

can be fabricated via the template-free hydrothermal method, which is simple, cost-effective, and environmentally friendly [18]. Furthermore, TiO_2 is a low-cost abundant resource known for its long-term stability, non-toxicity, and resistance to photo-corrosion.

Lanthanide ions have a special $4f^x5d^y$ electronic structure that enables them to form complexes with various compounds, such as TiO_2, that can donate a pair of nonbonding electrons. Incorporation of lanthanide ions in a TiO_2 matrix could concentrate organic pollutants on the surface and thus enhance electrocatalytic and/or photocatalytic activity [19] [20] [21] [22]. The specific surface area of the nanoscale catalyst and its particle size are very important parameters that strongly affect its catalytic activity.

In recent years, researchers used many Lanthanide elements to modify the TiO_2 nanostructure (such as La, Pr, Nd, Eu, Gd, Tb, Ho, Er and Yb) by different method to improve its photocatalytic and others applications [20]-[31]. In particular, Lanthanide elements (such as La, Eu, Gd and Ce) doped TNTs were prepared by hydrothermal method using NaOH to improve its photocatalytic and photoelectrocatalytic activity for oxidation of organic dye and organic compounds [20] [23] [29] [31]. Doping methods include wetness impregnation method [20], electrochemical anodization [21] [22] [27] [30], precipitation methods [24], sol-gel method [19] [25], hydrothermal treatment [26], wetness impregnation method [20], ultrasonic hydrothermal [29], ion exchange [31].

Here, the hydrothermal method for TNT syntheses and an *in-situ* doping strategy was used to incorporate Nd and/or Gd nanoparticles in TNT scaffolds. The effects of these lanthanides on the structural, textural, and morphological properties of TiO_2 nanomaterials obtained after calcination of hydrogen titanate nanotubes were investigated. The synthesized TNT, Nd and/or Gd-TNT show different applications, such as great performance of electro-oxidation of hydrazine by electrosensory [32] and determination of pharmaceutical compound as Alendronate sodium [33].

2. Experimental

2.1. Synthesis of TNTs

TiO_2 powder [P25, (99.5%, 21 nm)] and potassium hydroxide (KOH) were purchased from Sigma-Aldrich, USA. HCl for acid washing was purchased from S.D. Fine Chemicals, India. TNTs were synthesized via the hydrothermal method, where a mixture of 0.5 g of TiO_2 powder was dispersed in 30 mL of concentrated aqueous KOH solution. The mixture was stirred for 30 min and then transferred into a Teflon-lined stainless-steel autoclave, where the hydrothermal treatment was performed for 24 h at 150˚C [34]. The precipitate was collected and washed with deionized water and dilute HCl until the pH was 6.5. The TNTs were then dried for 10 h at 90˚C, followed by annealing at 400˚C for 2 h. In the case of doping, the molar ratio of titanium/dopant was 20:1 when $Nd(NO_3)_3$

and/or $Gd(NO_3)_3$ were added to the TiO_2 in the KOH solution. The hydrothermal and post-synthetic treatments were then performed as described above for the un-doped TNTs.

The samples were accordingly labelled TNTs, Nd-TNTs, Gd-TNTs, and Nd-Gd-TNTs. Finally, the TNTs became a white powder after drying and grinding. They were characterized with respect to surface morphology and crystallographic structure.

2.2. Apparatus

2.2.1. Morphology and Compound Composition

The morphological characterization of un-doped TNTs and doped TNTs prepped by hydrothermal method was achieved using Transmission Electron Microscope (TEM, JEOL JEM 1400, Japan) at 110 kV. The samples were prepared by dropping the ethanol solution of TNTs and Nd-TNTs, Gd-TNTs and Nd-Gd-TNTs catalysts on the Cu coating by carbon grids. The scanning electron microscopy (SEM) images were taken at different magnifications, without coating with conductive material, by (SEM, Super scan SS-550, Shimadzu, Japan). EDX was used to characterize the distribution of elements in un-doped TNTs and doped-TNTs synthesis by both hydrothermal using (EDX, Superscan SS-550, Shimadzu, Japan).

2.2.2. Crystalline Phase

Crystalline phases were acquired via X-ray diffraction (XRD, Shimadzu, XRD-7000, Japan) at 40 kV and 30 mA, using a Cu Kα incident beam (0.154 nm). The TNT molecular structures were characterized with Fourier-transform infrared spectroscopy (FT-IR, Thermo Fisher Scientific Inc., Madison, WI, USA) over the range 400 - 4000 cm^{-1}. Raman spectroscopy was performed with 532-nm excitation on a Raman microscope (Sentrarra, Bruker, USA) coupled to a Leica microscope (Olympus BX series, USA). The spectra were analyzed over the range 50 - 1200 cm^{-1}, with Rayleigh rejection via a 532 nm.

2.2.3. Surface Area and Porosity

Brunauer-Emmett-Teller specific surface areas (S_{BET}) of the TNTs were determined by a multipoint method using adsorption data for a relative pressure of 0.1515 (Micromeritics analyzer, Gemini VII, 2390 Surface Area and Porosity, USA).

3. Results and Discussion

3.1. Nanotube Morphologies

In **Figure 1(a)**, a spherical shape was observed for the P25 TiO_2 powder. The un-doped TNTs samples calcined at 400˚C (**Figure 1(b)**) were aggregated thread networks. **Figures 1(c)-(e)** are SEM images of in situ lanthanide-doped TNTs calcined at 400˚C. These nanotubes were heavily aggregated.

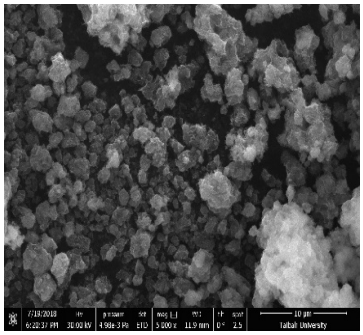

(a)

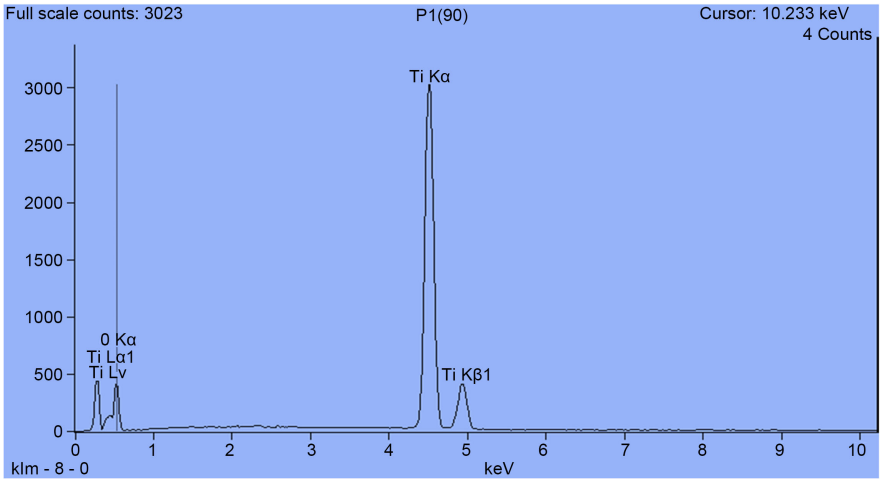
Full scale counts: 3023
P1(90)
Cursor: 10.233 keV
4 Counts
Ti Kα
0 Kα
Ti Lα1
Ti Lv
Ti Kβ1
klm - 8 - 0
keV

(a')

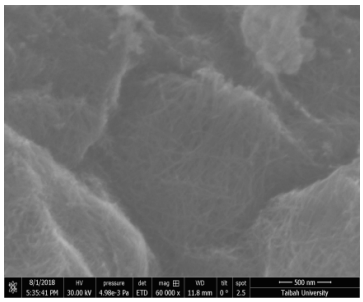

(b)

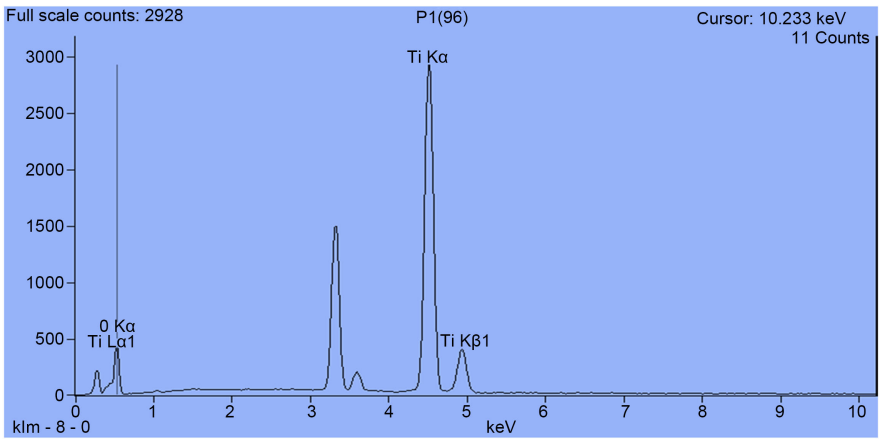
Full scale counts: 2928
P1(96)
Cursor: 10.233 keV
11 Counts
Ti Kα
0 Kα
Ti Lα1
Ti Kβ1
klm - 8 - 0
keV

(b')

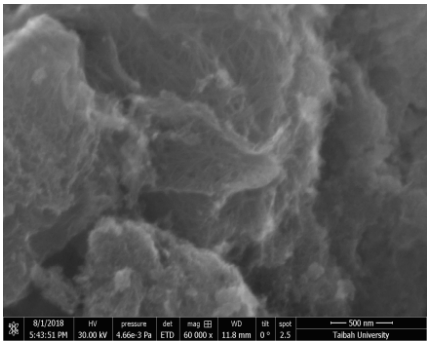

(c)

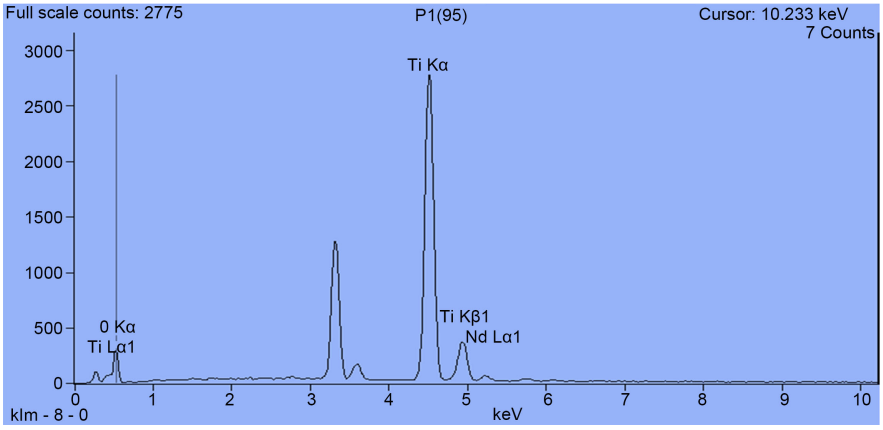
Full scale counts: 2775
P1(95)
Cursor: 10.233 keV
7 Counts
Ti Kα
Ti Kβ1
Nd La1
0 Kα
Ti La1
keV
klm - 8 - 0

(c')

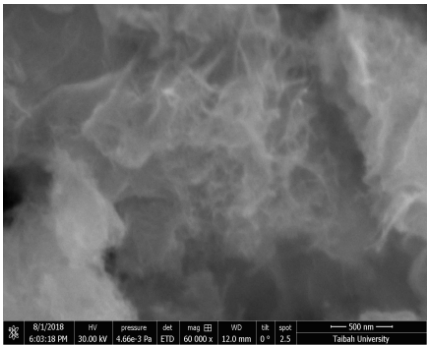

(d)

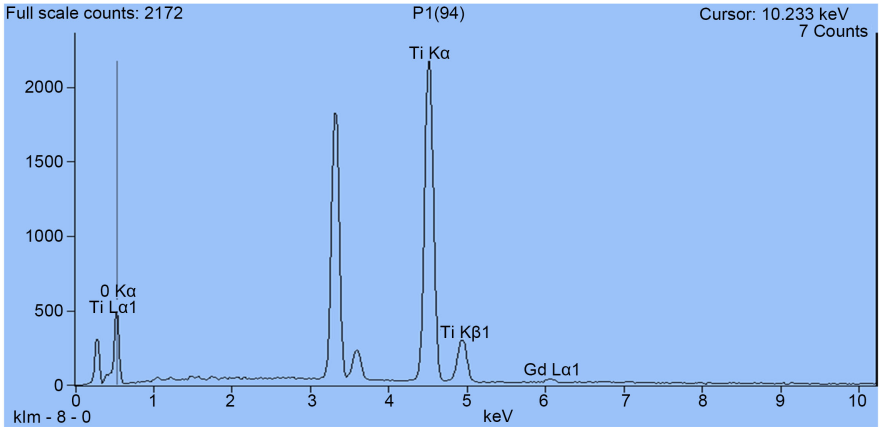
Full scale counts: 2172
P1(94)
Cursor: 10.233 keV
7 Counts
Ti Kα
Ti Kβ1
Gd La1
0 Kα
Ti La1
keV
klm - 8 - 0

(d')

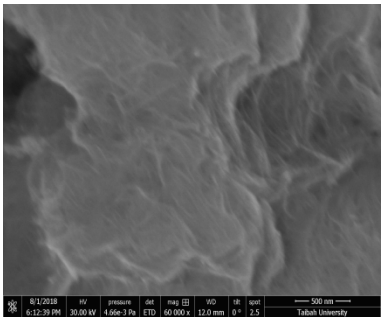

(e)

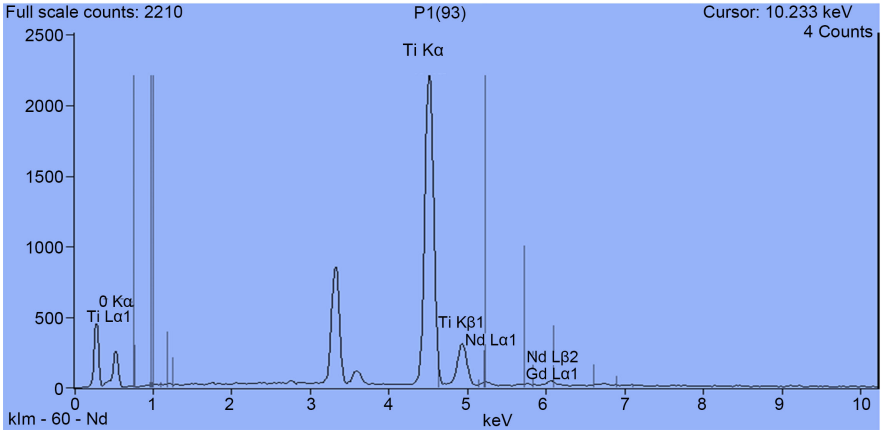

(e')

Figure 1. SEM images of ((a), (b), (c), (d)) P25 TiO_2 Powder, undoped TNTs, Nd-TNTs, Gd-TNTs, and Nd-Gd-TNTs; ((a'), (b'), (c'), (d')) EDX of undoped TNTs, Nd-TNTs, Gd-TNTs, and Nd-Gd-TNTs respectively.

The approximate compositions of P25 and the un-doped and doped TNTs were calculated from EDX spectra (**Figures 1(a')-(e')**). Uniform distributions of Nd and Gd nanoparticles were observed in the TNT lattice. As shown in **Table 1**, the EDX patterns had nearly 3.37% Nd loading in the Nd-TNTs, 2.92% Gd loading in the Gd-TNTs, and 9.42% Nd and 3.48% Gd loading in the Nd-Gd TNTs.

Figure 2(a) displays a TEM image of un-doped TNTs that were aggregated and formed a large composite fiber-like structure, in agreement with the SEM images. The nanotubes were uniform and hollow, with multiwall sheets. The outer diameters were 6.5 - 10.6 nm, and the lengths were 51 nm. The open-ended fiber-like structures of uniform, multiwall, straight tubes are shown in **Figures 2(b)-(d)**. The well-dispersed Nd and/or Gd oxide nanoparticles in the TNT lattice also can be seen. The outer diameter of the Nd-TNT multi-layered sheets was in the range of 5.7 - 8 nm, that for the Gd-TNTs was in the range of 6.1 - 14.2 nm, and that for the Nd-Gd-TNTs was in range of 9.4 nm - 14.2 nm.

The mechanisms for multiwall TNT formation by hydrothermal treatment could be understood as follows. When the Ti precursors were mixed with the concentrated aqueous KOH at high temperature and pressure, Ti-O-K bonds formed on the TiO_2 surface instead of "Ti-O-Ti" bonds because of the concentrated KOH [35]. These salts formed nanosheets by:

Table 1. EDX analysis of P25 TiO_2, undoped TNTs, Lanthanides-doped TNTs.

Spectrum Label	O%	Ti%	Nd%	Gd%	Total
P25 TiO_2	46.56	53.44	---	---	100.00
Undoped TNTs	49.07	50.93	---	---	100.00
Nd-TNTs	40.97	55.66	3.37	---	100.00
Gd-TNTs	53.55	43.53	---	2.92	100.00
Nd-Gd-TNTs	41.72	45.38	9.42	3.48	100.00

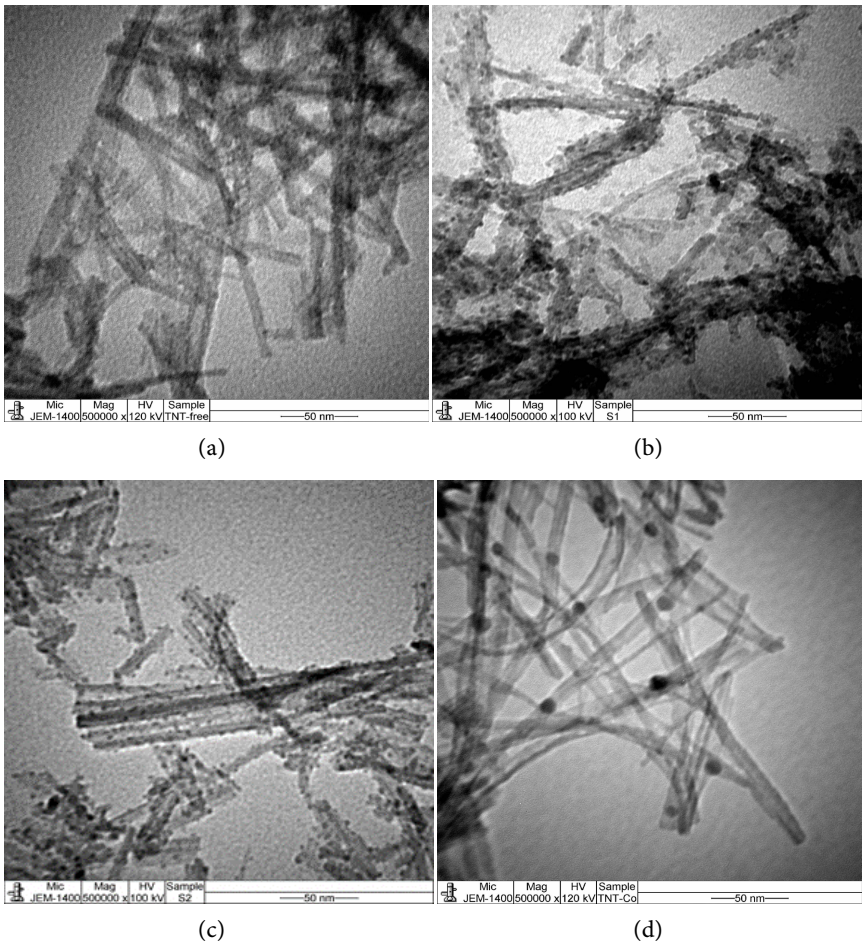

(a) (b)

(c) (d)

Figure 2. TEM images of (a) undoped TNTs, (b) Nd-TNTs, (c) Gd-TNTs, and (d) Nd-Gd-TNTs.

$$\text{Ti-O-Ti} + 2\text{KOH} \rightarrow 2\left(\text{Ti-O}^{-}, \text{K}^{+}\right) + \text{H}_2\text{O} \tag{1}$$

Then, when the samples were treated with deionized water, the Ti-O-K bonds in the $\left(\text{K}_2\text{Ti}_n\text{O}_{2n+1}\right)$ multilayer crystal gradually converted into Ti-OH bonds in sheets of hydroxyl titanate $\left(\text{H}_2\text{Ti}_n\text{O}_{2n+1}\right)$. After the sample was treated by dilute acid, Ti-O-Ti bonds [36] or Ti-O-H···O-Ti hydrogen bonds were generated according to:

$$\left(\text{Ti-O}^{-}, \text{K}^{+}\right) + \text{H}^{+} \rightarrow \text{Ti-OH} + \text{K}^{+} \tag{2}$$

These bonds significantly decreased the Ti-O length, thus leading to the folding of the sheets into a multiwall tube structure, as shown in Figure 3.

3.2. Crystalline Phase Characterization

The crystal phases of P25 TiO_2 and un-doped and doped TNTs are shown in Figure 4. The XRD patterns in Figure 4(e) for P25 TiO_2 indicated anatase phase planes with main peaks located at 25.3˚, 37.8˚, 48.0˚, and 55.1˚, respectively corresponding to the (101), (004), (200), and (211) planes, in good convention with the standard spectrum [Joint Committee on Powder Diffraction Standards (JCPDS), card no.: 21-1272] [37]. The XRD patterns of un-doped TNTs are shown in Figure 4(a), where diffraction peaks were observed at 24.90˚, 48.10˚, and 55.91˚, corresponding to the (101), (200), and (211) crystal planes of anatase TiO_2, respectively. These data suggested an anatase phase of TiO_2 (JCPDS, card no.: (00-021-1272). However, these XRD patterns were typical of layered materials, suggesting that the TNTs were multi-walled [38]. The diffraction peak with a low 2θ value of 11.5˚ (020) corresponded to the TNT interlayer distance. An intense peak at $2\theta = 48.10$˚ was due to the edge-sharing TiO_6 octahedral [18].

The diffraction planes of anatase in Figure 4(b) were sharp, indicating good crystallization of Nd-TNTs, and the other four peaks had the same positions of 22.70˚, 32.45˚, 46.65˚, and 57.28˚ assigned to (002), (200), (220), and (132) reflections, indicating well-embedded incorporation of Nd ions in the TiO_2 lattice as $NdTiO_3$ (JCPDS, card no.: (00-029-0922). Meanwhile, in Figure 4(c), there were characteristic peaks of Gd observed at 29.28˚, 31.64˚, 47.89˚, and 58.72˚ assigned to (201), (040), (341), and (611) planes, respectively, indicating Gd ions in the form of Gd_2TiO_5 (JCPDS, card no.: (00-021-0342). The XRD patterns recorded for co-doped Nd-Gd-TNTs are shown in Figure 4(d). They revealed anatase phases, with new peaks for Nd and/or Gd.

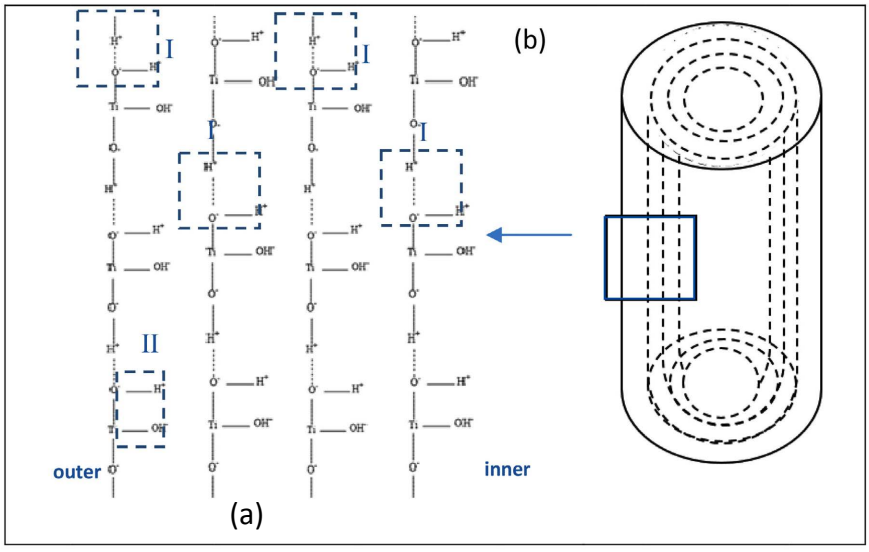

Figure 3. Hydroxyl titanate nanosheets ($H_2Ti_nO_{2n+1}$), (a) mechanism for breaking of $Na_2Ti_2O_4(OH)_2$, (b) rolling up the nanosheet to nanotubes.

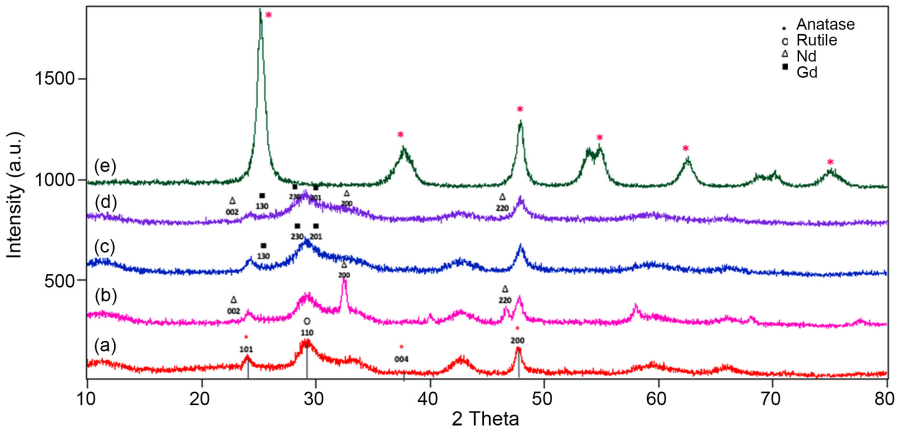

Figure 4. XRD image of (a) P25 TiO_2, (b) undoped TNTs, (c) Nd-TNTs, (d) Gd-TNTs, and (e) Nd-Gd-TNTs.

The occasional absence of sharp peaks corresponding to Nd and/or Gd in the XRD patterns could be attributed to small or highly dispersed concentrations below the detection limit, or they were located inside the TiO_2 lattice (*i.e.*, TNT doping) [39].

Grain sizes of the P25 TiO_2 and the un-doped and doped TNT powders were calculated using the Scherrer equation. The crystalline sizes are shown in **Table 2**, where there was a slight change when Nd and/or Gd were incorporated.

The slight expansion of the TiO_2 crystal volume after lanthanide modification suggested that the Nd and Gd oxide were located at the crystal boundaries rather than inside the TiO_2 unit cell [38] [39]. For the Nd-Gd-TNTs, the crystallite size was reduced from 7.06 nm to 6.35 nm. Zhang *et al.* [40] and Meksi *et al.* [20] explained this decrease of the TiO_2 anatase phase in terms of dopant cations located at the grain boundary hindering grain growth.

3.3. BET Surface Area

The BET surface area in **Table 2** of un-doped TNTs was 160 m^2/g, which increased to 175 m^2/g for (20:1) for Nd-loading, 207 m^2/g for (20:1) Gd-loading, and 231 m^2/g (20:1) for Nd-Gd-loading. The massive increases compared to P25 were attributed to the tubular form of the TNTs [41]. The doped TNTs had a larger mesoporous volume than that of the undoped TNTs, while no change was observed in pore size. The larger mesoporous volume of all rare-earth-loaded TNTs samples has been attributed to the enhanced mesoporosity [40].

3.4. Resonance Raman Spectra

A Raman spectrum of un-doped TNTs is shown in **Figure 5**. The peaks observed in **Table 3** at 143 cm^{-1} (E_{1g}), 198 cm^{-1} (E_{2g}), 394 cm^{-1} (B_{1g}), and 638 cm^{-1} (E_{3g}) were attributed to anatase TiO_2, in agreement with previous studies [42] [43] [44]. The strongest E_{1g} mode at 143 cm^{-1}, attributed to the external vibration of the anatase structure, was well resolved and indicated that the anatase phase was formed in the nanotube [45]. This was in good agreement with the XRD data and

previous work. The E_g peak was attributed mainly to the symmetric stretching vibration of O-Ti-O linkages in TiO_2, the symmetric bending vibration of O-Ti-O was confirmed by B_{1g}, and the A_{1g} peak was associated with the antisymmetric bending vibration of the O-Ti-O linkage [33]. The same strong peaks observed in Figures 5(b)-(d) for the doped TNTs had anatase characteristics, indicating that Nd and Gd may be introduced into the lattice or interstitial sites of TiO_2.

Table 2. Particle sizes, BET surface area, pore volume and pore size of synthesis TNTs

Sample	Average Crystalline Size (nm)	BET Specific Surface Area, S_{BET} (m^2/g)	Pore Volume ($cm^3 \cdot g^{-1}$)	Pore Size (˚A)
P25 TiO_2	7.31	58.90	0.047	16.9
Undoped TNTs	7.06	160	0.064	16.05
Nd-TNTs (Ti:Nd = 20:1)	7.93	175	0.068	16.07
Gd-TNTs (Ti:Gd = 20:1)	7.91	207	0.083	16.06
Nd-Gd-TNTs (Ti:Nd + Gd = 20:1)	6.35	231	0.073	16.11

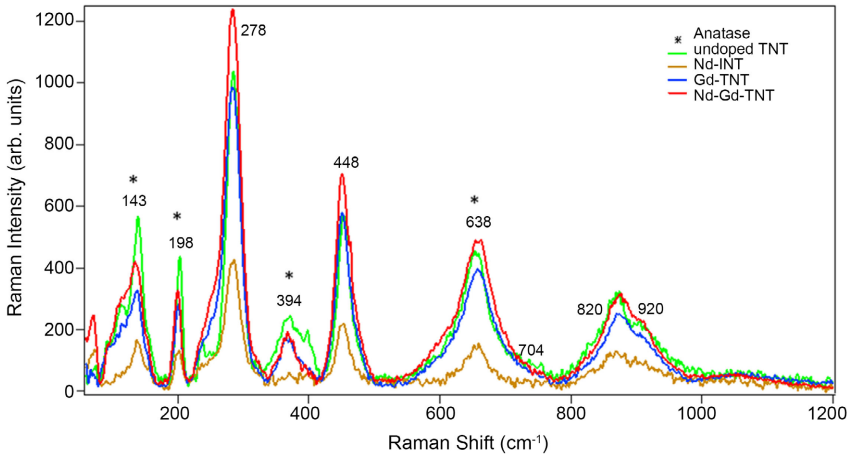

(A)

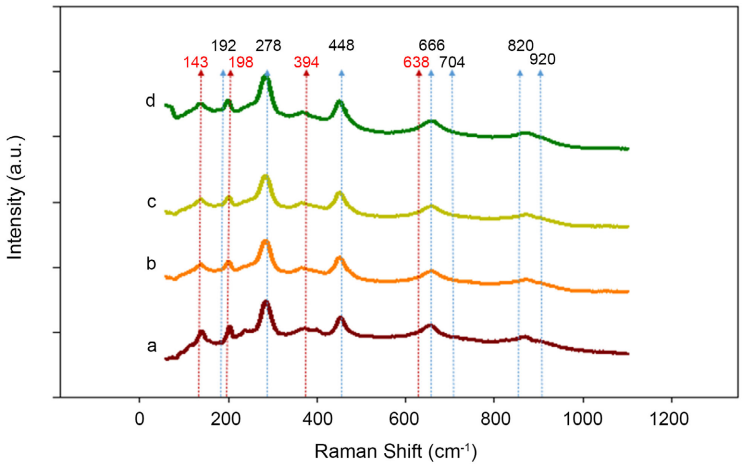

(B)

Figure 5. Raman spectra of (a) undoped TNTs, (b) Nd-TNTs, (c) Gd-TNTs, and (d) Nd-Gd-TNTs.

Table 3. Raman shift of vibration mode for different catalyst supports.

Raman shift (cm^{-1})	Vibration	Ref.
143	symmetric stretching vibration of O-Ti-O in anatase form	[45]
198	symmetric stretching vibration of Ti-O-Ti in anatase form	[43] [46]
278	symmetric stretching vibration of Ti-O-K bonds	[50]
394	symmetric binding vibration of Ti-O-Ti in anatase form	[42]
448	symmetric stretching vibration of Ti-O-Ti crystal phonons	[46]
638	symmetric stretching vibration of Ti-O-Ti crystal phonons	[46]
704	symmetric stretching vibration of covalent Ti-O-H bonds	[46]
820	symmetric stretching vibration of covalent Ti-O-H bonds	[47]
920	surface Ti-O-K vibrations	[47]

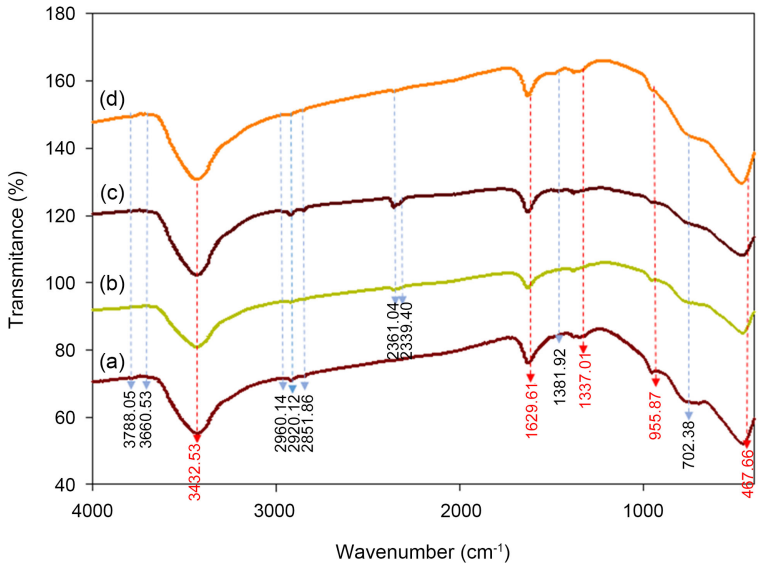

Figure 6. FT-IR spectroscopy of (a) TNTs, (b) Nd-TNTs, (c) Gd-TNTs, and (d) Nd-Gd -TNTs.

The band at 278 cm^{-1} was assigned to the stretching vibration of Ti-O-K bonds [45], while the bands at 198 cm^{-1} and 394 cm^{-1} corresponded to anatase Ti-O-Ti [43]. The bands at 448 cm^{-1} were related to Ti-O-Ti crystal phonons [46]. The bands at 704 cm^{-1} and 820 cm^{-1} corresponded to covalent Ti-O-H bonds, and the band at 920 cm^{-1} was assigned to surface Ti-O-K vibrations [47] (**Table 3**).

3.5. Fourier-Transform Infrared Spectra

In FT-IR spectra of TNTs (**Figure 6**), three absorption bands cantered at 3432.53 cm^{-1}, 1627.87 cm^{-1}, and 955.87 cm^{-1} were assigned to stretching vibrations of OH groups, and bending vibrations of H-O-H and Ti-O bonds, respectively [48]. The strong intensity of the hydroxyl groups at 3432.53 cm^{-1} indicated a large concentration on the un-doped TNT surface. This helped conjunction and

dispersion of the metal particles on the TNT walls [49] [50] [51] [52], and also captured photoexcited electrons and holes to produce reactive oxygen species for photocatalysis of organic wastewater. The peaks at 1627.87 cm^{-1} and 1349.52 cm^{-1} corresponded to undoped TNTs [50]. The unchanged intensity of the 3432.53 cm^{-1} band may have been due to the interactions of doped Nd and Gd in the TiO_2 lattice that did not replace -OH groups on the oxide surface. Moreover, the band at 446 ± 4 cm^{-1} corresponded to the asymmetric vibration of M-Ti-O (M = K, Nd, Gd) groups inside the lattice [27]. In all cases, the FT-IR spectra kept their general features, which confirmed that the metals and the TNTs had strong chemical interactions, consistent with the XRD and Raman structural analyses.

4. Conclusion

The fabrication of un-doped TNTs and Nd- and/or Gd-doped TNTs was demonstrated via the environmentally-friendly hydrothermal treatment of TiO_2 P25 in a concentrated KOH solution and *in-situ* doping. The morphologies of all the samples from SEM, EDX, and TEM data confirmed that the structure of the multiwall nanotubes was fiber-like with a uniform distribution of Nd and/or Gd ions in the TNT lattice. The nanotubes were in an anatase phase, even after doping with Nd and/or Gd oxide. The mixed Nd-Gd-TNTs had smaller grain sizes because the dopant cations were located at the grain boundary, thus hindering grain growth. It was found that the specific surface area of the nanotubes (50 - 210 m^2/g) considerably exceeded that of the initial TiO_2 (12 m^2/g).

Acknowledgements

The authors thank Prof. Abdullah Al-Mayouf from King Saud University for his helpful advice on various technical issues. In addition, the authors would like to thank the technicians, Mr. Abdallah Jaber (physics department) and Miss. Fatemah Abdalraheem (chemistry department) for conducting surface measurements of the study samples.

Contribution

Emran and Alanazi carried out the experiments. Emran developed the theory and performed the computations with Alanazi. Emran encouraged Alanazi to investigate the preparation of TNTA and supervised the findings of this work. Both authors discussed the results and contributed to the final manuscript.

Conflicts of Interest

The authors declare no conflicts of interest regarding the publication of this paper.

References

[1] Madian, M., Eychmüller, A. and Giebeler, L. (2018) Current Advances in TiO_2-Based Nanostructure Electrodes for High Performance Lithium Ion Batteries. *Batteries*, **4**,

Article No. 7. https://doi.org/10.3390/batteries4010007

[2] Beydoun, D., Amal, R., Low, G. and McEvoy, S. (1999) Role of Nanoparticles in Photocatalysis. *Journal of Nanoparticle Research*, **1**, 439-458. https://doi.org/10.1023/A:1010044830871

[3] Clarizia, L., Russo, D., Di Somma, I., *et al.* (2018) Multifunctional Photocatalytic Materials for Energy. Woodhead Publishing, Sawston.

[4] Wang, W., Li, G., Xia, D., et al. (2017) Photocatalytic Nanomaterials for Solar-Driven Bacterial Inactivation: Recent Progress and Challenges. Environmental Science: *Nano*, **4**, 782-799. https://doi.org/10.1039/C7EN00063D

[5] Wang, X., Li, X., Liu, D., *et al.* (2012) Highly Luminescent Carbon Nanodots by Microwave-Assisted Pyrolysis. *Chemical Communications*, **48**, 7955-7957. https://doi.org/10.1039/c2cc33869f

[6] Mahmood, A., Guo, W., Tabassum, H. and Zou, R. (2016) Metal-Organic Framework-Based Nanomaterials for Electrocatalysis. *Advanced Energy Materials*, **6**, Article ID: 1600423. https://doi.org/10.1002/aenm.201600423

[7] Byranvand, M.M., Kharat, A.N. and Bazargan, M.H. (2012) Titania Nanostructures for Dye-Sensitized Solar Cells. *Nano-Micro Letters*, **4**, 253-266. https://doi.org/10.1007/BF03353723

[8] Salari, M., Aboutalebi, S.H., Aghassi, A., *et al.* (2015) Disorder Engineering of Undoped TiO_2 Nanotube Arrays for Highly Efficient Solar-Driven Oxygen Evolution. *Physical Chemistry Chemical Physics*, **17**, 5642-5649. https://doi.org/10.1039/C4CP03177F

[9] Lee, Y.-L., Chi, C.-F. and Liau, S.-Y. (2009) CdS/CdSe Co-Sensitized TiO_2 Photoelectrode for Efficient Hydrogen Generation in a Photoelectrochemical Cell. *Chemistry of Materials*, **22**, 922-927. https://doi.org/10.1021/cm901762h

[10] Guayaquil-Sosa, J.F., Calzada, A., Serrano, B., Escobedo, S. and de Lasa, H. (2017) Hydrogen Production via Water Dissociation Using Pt-TiO_2 Photocatalysts: An Oxidation-Reduction Network. *Catalysts*, **7**, 324-345. https://doi.org/10.3390/catal7110324

[11] Naldoni, A., Altomare, M., Zoppellaro, G., *et al.* (2018) Photocatalysis with Reduced TiO_2: From Black TiO_2 to Cocatalyst-Free Hydrogen Production. *ACS Catalysis*, **9**, 345-364. https://doi.org/10.1021/acscatal.8b04068

[12] Song, Y.-Y., Schmidt-Stein, F., Bauer, S. and Schmuki, P. (2009) Amphiphilic TiO_2 Nanotube Arrays: An Actively Controllable Drug Delivery System. *Journal of the American Chemical Society*, **131**, 4230-4232. https://doi.org/10.1021/ja810130h

[13] Wang, T., Jiang, H., Wan, L., *et al.* (2015) Potential Application of Functional Porous TiO_2 Nanoparticles in Light-Controlled Drug Release and Targeted Drug Delivery. *Acta Biomaterialia*, **13**, 354-363. https://doi.org/10.1016/j.actbio.2014.11.010

[14] Enachi, M., Guix, M., Braniste, T., *et al.* (2015) Photocatalytic Properties of TiO_2 Nanotubes Doped with Ag, Au and Pt or Covered by Ag, Au and Pt Nanodots. *Surface Engineering and Applied Electrochemistry*, **51**, 3-8. https://doi.org/10.3103/S1068375515010044

[15] Perera, S.D., Mariano, R.G., Vu, K., *et al.* (2012) Hydrothermal Synthesis of Graphene-TiO_2 Nanotube Composites with Enhanced Photocatalytic Activity. *ACS Catalysis*, **2**, 949-956. https://doi.org/10.1021/cs200621c

[16] Lei, B., Xue, J.J., Jin, D.P., *et al.* (2008) Fabrication, Annealing, and Electrocatalytic Properties of Platinum Nanoparticles Supported on Self-Organized TiO_2 Nanotubes. *Rare Metals*, **27**, 445-450. https://doi.org/10.1016/S1001-0521(08)60160-6

[17] Zhang, Q., Wei, Y., Wang, Y., *et al.* (2017) Fabrication and Electrocatalytic Activity of TiO_2 Nanotubes Based Electrode with High Oxygen Evolution Potential. *Journal of Nanoscience and Nanotechnology*, **17**, 1950-1956. https://doi.org/10.1166/jnn.2017.12935

[18] Liu, N., Chen, X., Zhang, J. and Schwank, J.W. (2014) A Review on TiO_2-Based Nanotubes Synthesized via Hydrothermal Method: Formation Mechanism, Structure Modification, and Photocatalytic Applications. *Catalysis Today*, **225**, 34-51. https://doi.org/10.1016/j.cattod.2013.10.090

[19] Reszczyńska, J., Grzyb, T., Sobczak, J.W., *et al.* (2014) Lanthanide Co-Doped TiO_2: The Effect of Metal Type and Amount on Surface Properties and Photocatalytic Activity. *Applied Surface Science*, **307**, 333-345. https://doi.org/10.1016/j.apsusc.2014.03.199

[20] Meksi, M., Turki, A., Kochkar, H., *et al.* (2016) The Role of Lanthanum in the Enhancement of Photocatalytic Properties of TiO_2 Nanomaterials Obtained by Calcination of Hydrogenotitanate Nanotubes. *Applied Catalysis B*: *Environmental*, **181**, 651-660. https://doi.org/10.1016/j.apcatb.2015.08.037

[21] Mazierski, P., Lisowski, W., Grzyb, T., *et al.* (2017) Enhanced Photocatalytic Properties of Lanthanide-TiO_2 Nanotubes: An Experimental and Theoretical Study. *Applied Catalysis B*: *Environmental*, **205**, 376-385. https://doi.org/10.1016/j.apcatb.2016.12.044

[22] Parnicka, P., Mazierski, P., Lisowski, W., *et al.* (2018) A New Simple Approach to Prepare Rare-Earth Metals-Modified TiO_2 Nanotube Arrays Photoactive under Visible Light: Surface Properties and Mechanism Investigation. *Results in Physics*, **12**, 412-423. https://doi.org/10.1016/j.rinp.2018.11.073

[23] Li, H., Sheng, Y., Zhang, H., *et al.* (2011) Synthesis and Luminescent Properties of TiO_2:Eu^{3+} Nanotubes. *Powder Technology*, **212**, 372-377. https://doi.org/10.1016/j.powtec.2011.06.019

[24] Hewer, T.L.R., Souza, E.C.C., Martins, T.S., Muccillo, E.N.S. and Freire, R.S. (2011) Influence of Neodymium Ions on Photocatalytic Activity of TiO_2 Synthesized by Sol-Gel and Precipitation Methods. *Journal of Molecular Catalysis A*: *Chemical*, **336**, 58-63. https://doi.org/10.1016/j.molcata.2010.12.010

[25] Nassoko, D., Li, Y.-F., Li, J.-L., Li, X. and Yu, Y. (2012) Neodymium-Doped TiO_2 with Anatase and Brookite Two Phases: Mechanism for Photocatalytic Activity Enhancement under Visible Light and the Role of Electron. *International Journal of Photoenergy*, **2012**, Article ID: 716087. https://doi.org/10.1155/2012/716087

[26] Li, L., Zhou, Z., Lei, J., He, J., Liu, P. and Pan, F. (2012) Nd_2O_3-Decorated TiO_2 Nanotube Arrays with High Photoelectrocatalytic Activity. *Materials Letters*, **79**, 252-255. https://doi.org/10.1016/j.matlet.2012.04.017

[27] Nie, J., Mo, Y., Zheng, B., Yuan, H. and Xiao, D. (2013) Electrochemical Fabrication of Lanthanum-Doped TiO_2 Nanotube Array Electrode and Investigation of Its Photoelectrochemical Capability. *Electrochimica Acta*, **90**, 589-596. https://doi.org/10.1016/j.electacta.2012.12.049

[28] Zheng, Y. and Wang, W. (2014) Electrospun Nanofibers of Er^{3+}-Doped TiO_2 with Photocatalytic Activity beyond the Absorption Edge. *Journal of Solid State Chemistry*, **210**, 206-212. https://doi.org/10.1016/j.jssc.2013.11.029

[29] Chai, Y., Lin, L., Zhang, K., Zhao, B. and He, D. (2014) Efficient Visible-Light Photocatalysts from Gd-La Codoped TiO_2 Nanotubes. *Ceramics International*, **40**, 2691-2696. https://doi.org/10.1016/j.ceramint.2013.10.054

[30] Wang, X., Jia, H., Wang, Y., Li, Y. and Bao, Z. (2016) The Photocatalytic Perfor-

mance Research of La_2O_3 Modified TiO_2 Nanotube Arrays. *Journal of Materials Science: Materials in Electronics*, **27**, 7073-7078. https://doi.org/10.1007/s10854-016-4665-4

[31] Tuyen, L.T.T., Quang, D.A., Toan, T.T.T., *et al.* (2018) Synthesis of CeO_2/TiO_2 Nanotubes and Heterogeneous Photocatalytic Degradation of Methylene Blue. *Journal of Environmental Chemical Engineering*, **6**, 5999-6011. https://doi.org/10.1016/j.jece.2018.09.022

[32] Emran, K.M., Ali, S.M. and Alanazi, H.E. (2020) Novel Hydrazine Sensors Based on Pd Electrodeposited on Highly Dispersed Lanthanide-Doped TiO_2 Nanotubes. *Journal of Electroanalytical Chemistry*, **856**, Article ID: 113661. https://doi.org/10.1016/j.jelechem.2019.113661

[33] Amro, A.N., Emran, K.M. and Alanazi, H.E. (2020) Voltammetric Determination of Itopride Using Carbon Paste Electrode Modified with Gd Doped TiO_2 Nanotubes. *Journal of Chemistry*, **44**, 1122-1133. https://doi.org/10.3906/kim-2003-56

[34] Emran, K.M. (2020) Catalytic Activity of Strontium Modified TiO_2 Nanotubes for Hydrogen Evolution Reaction. *International Journal of Electrochemical Science*, **15**, 4218-4231. https://doi.org/10.20964/2020.05.02

[35] Harsha, N., Ranya, K.R., Babitha, K.B., *et al.* (2011) Effect of Silver and Palladium on Dye-Removal Characteristics of Anatase-Titania Nanotubes. *Journal of Nanoscience and Nanotechnology*, **11**, 1175-1187. https://doi.org/10.1166/jnn.2011.3048

[36] Zhang, S., Li, W., Jin, Z., *et al.* (2004) Study on ESR and Inter-Related Properties of Vacuum-Dehydrated Nanotubed Titanic Acid. *Journal of Solid State Chemistry*, **177**, 1365-1371. https://doi.org/10.1016/j.jssc.2003.11.027

[37] Ohno, T., Sarukawa, K., Tokieda, K. and Matsumura, M. (2001) Morphology of a TiO_2 Photocatalyst (Degussa, P-25) Consisting of Anatase and Rutile Crystalline Phases. *Journal of Catalysis*, **203**, 82-86. https://doi.org/10.1006/jcat.2001.3316

[38] Alves, W., Ribeiro, A.O., Pinheiro, M.V.B., *et al.* (2011) Quenching of Photoactivity in Phthalocyanine Copper(II)-Titanate Nanotube Hybrid Systems. *The Journal of Physical Chemistry C*, **115**, 12082-12089. https://doi.org/10.1021/jp202101r

[39] Parnicka, P., Mazierski, P., Grzyb, T., *et al.* (2018) Influence of the Preparation Method on the Photocatalytic Activity of Nd-Modified TiO_2. *Beilstein Journal of Nanotechnology*, **9**, 447-459. https://doi.org/10.3762/bjnano.9.43

[40] Zhang, Y., Zhang, H., Xu, Y. and Wang, Y. (2004) Significant Effect of Lanthanide Doping on the Texture and Properties of Nanocrystalline Mesoporous TiO_2. *Journal of Solid State Chemistry*, **177**, 3490-3498. https://doi.org/10.1016/j.jssc.2004.05.026

[41] Subramaniam, M.N., Goh, P.S., Ismail, A.F. and Lau, W.J. (2016) Effect of Titania Nanotubes on the Flux and Separation Performance of Polyethersulfone Membranes. *IOP Conference Series: Earth and Environmental Science*, **36**, Article ID: 012024. https://doi.org/10.1088/1755-1315/36/1/012024

[42] Huang, S., Si, Z., Li, X., *et al.* (2016) A Novel Au/R-GO/Tnts Electrode for H_2O_2, O_2 and Nitrite Detection. *Sensors and Actuators B: Chemical*, **234**, 264-272. https://doi.org/10.1016/j.snb.2016.04.167

[43] Van Viet, P., Phan, B.T., Mott, D., Maenosono, S., Sang, T.T. and Thi, C.M. (2018) Silver Nanoparticle Loaded TiO_2 Nanotubes with High Photocatalytic and Antibacterial Activity Synthesized by Photoreduction Method. *Journal of Photochemistry and Photobiology A: Chemistry*, **352**, 106-112. https://doi.org/10.1016/j.jphotochem.2017.10.051

[44] Tahir, B., Tahir, M. and Amin, N.A.S. (2018) Tailoring Performance of La-Modified TiO_2 Nanocatalyst for Continuous Photocatalytic CO_2 Reforming of CH_4 to Fuels in

the Presence of H_2O. *Energy Conversion and Management*, **159**, 284-298. https://doi.org/10.1016/j.enconman.2017.12.089

[45] Ali, I. and Kim, J.O. (2018) Visible-Light-Assisted Photocatalytic Activity of Bismuth-TiO_2 Nanotube Composites for Chromium Reduction and Dye Degradation. *Chemosphere*, **207**, 285-292. https://doi.org/10.1016/j.chemosphere.2018.05.075

[46] Zhang, S.P., Lin, J.S, Lin, R.K., *et al*. (2020) *In Situ* Raman Study of the Photoinduced Behavior of Dye Molecules on TiO_2 (hkl) Single Crystal Surfaces. *Chemical Science*, **11**, 6431-6435. https://doi.org/10.1039/D0SC00588F

[47] Monção, M.M., Barreto, I.C., Miguel, F.B., *et al*. (2022) Raman Spectroscopy Analysis of Wollastonite/Tricalcium Phosphate Glass-Ceramics after Implantation in Critical Bone Defect in Rats. *Materials Sciences and Applications*, **13**, 317-333. https://doi.org/10.4236/msa.2022.135017

[48] Dong, B., He, B.-L., Huang, J., Gao, G.-Y., Yang, Z. and Li, H.-L. (2008) High Dispersion and Electrocatalytic Activity of Pd/Titanium Dioxide Nanotubes Catalysts for Hydrazine Oxidation. *Journal of Power Sources*, **175**, 266-271. https://doi.org/10.1016/j.jpowsour.2007.08.090

[49] Dong, B., He, B., Chai, Y. and Liu, C. (2010) Novel Pt Nanoclusters/Titanium Dioxide Nanotubes Composites for Hydrazine Oxidation. *Materials Chemistry and Physics*, **120**, 404-408. https://doi.org/10.1016/j.matchemphys.2009.11.022

[50] Wang, Y.-F., Peng, C.-F. and Chao, H.-P. (2015) Sorption of Volatile Organic Compounds on Organic Substance-Modified Titanate Nanotubes. *Aerosol and Air Quality Research*, **15**, 2688-2699. https://doi.org/10.4209/aaqr.2015.10.0592

[51] Qu, X.F., Yuan, J.J., Da Deng, X., Hou, Y.C., Wang, Y.F. and Song, H.B. (2017) An Efficient Method to Form TiO_2/CdS Nanotube Arrays Using Anodic Aluminum Oxide (AAO) Templates. *Key Engineering Materials*, **727**, 374-380. https://doi.org/10.4028/www.scientific.net/KEM.727.374

[52] Zhao, F., Rong, Y., Wan, J., Hu, Z., Peng, Z. and Wang, B. (2018) High Photocatalytic Performance of Carbon Quantum Dots/TNTs Composites for Enhanced Photogenerated Charges Separation under Visible Light. *Catalysis Today*, **315**, 162-170. https://doi.org/10.1016/j.cattod.2018.02.019